Study of COVID-19 Epidemiological Evolution in India Using the Multi-Wave SIR Model

Mr. Krish Saraf

29 Oct, 2024

1 Introduction

The COVID-19 pandemic, triggered by the SARS-CoV-2 virus in December 2019, quickly spread worldwide, resulting in numerous infection waves. Multiple epidemiological peaks have been observed, with five successive waves documented in regions like the European Union, USA, Russia, and Canada, while countries such as India, Indonesia, and Brazil have experienced three distinct waves. Each country's infection peaks differ in width, height, and separation, indicating the unique characteristics of COVID-19 spread globally. This pattern is partly due to new variants that can cause reinfections, leading to multiple peaks within a single population.

To study the pandemic's dynamics, several models based on the classic SIR (Susceptible-Infected-Removed) model, introduced by Kermack and McKendrick in 1927, have been proposed. However, the original SIR model only predicts a single infection peak. Other models, such as SEIR and SIQR, extend the SIR framework to consider factors like quarantine and latency. These models have been applied to study COVID-19 patterns in various countries, yet a multi-wave approach to COVID-19 dynamics through a single deterministic model had not been established before. The MWSIR model achieves this by allowing a probability of reinfection, which aligns with the observed repeated infection waves.

2 SIR Model Overview

The classic SIR model divides the population into three compartments:

- **Susceptible (S)**: Individuals who are healthy but may contract the infection.
- **Infected (I)**: Individuals who are currently infected and can spread the disease.
- **Removed (R)**: Individuals who have recovered or succumbed to the disease and are no longer infectious.

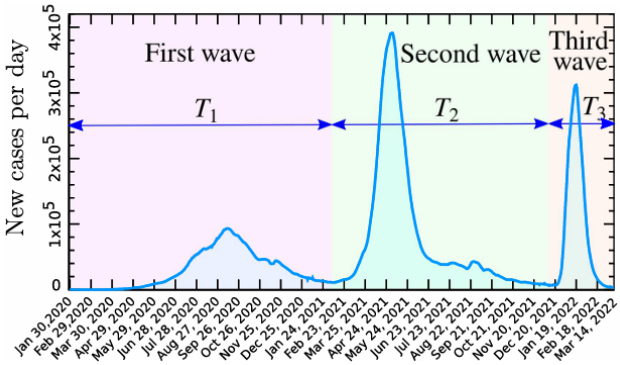

Figure 1: Daily new COVID-19 cases in terms of seven-day moving average in India during January 30, 2020 to March 14, 2022 (775 days).

The dynamics of these compartments are modeled by the following equations:

$$\frac{dS}{dt} = -\alpha SI, \quad \frac{dI}{dt} = \alpha SI - \beta I, \quad \frac{dR}{dt} = \beta I$$

where:

- α is the infection rate,
- β is the recovery rate.

This single-wave model yields a solitary infection peak, as S consistently declines over time.

3 Multi-Wave SIR (MWSIR) Model

To reflect multiple waves, the MWSIR model introduces a probability of re-infection after recovery. In this model, the total population is divided into Susceptible (S), Infected (I), and Removed (R) compartments. However, the recovered population has a probability, γ, of becoming susceptible again after a delay τ. The model's equations are:

$$\frac{dS}{dt} = \mu N - \alpha S(t)I(t) + \gamma I(t-\tau) - \mu S(t)$$

$$\frac{dI}{dt} = \alpha S(t)I(t) - \beta I(t) - \mu I(t)$$

$$\frac{dR}{dt} = \beta I(t) - \gamma I(t-\tau) - \mu R(t)$$

where:

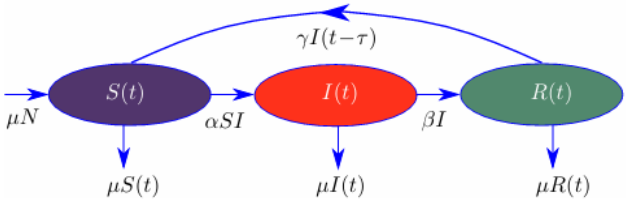

Figure 2: Flowchart for the MWSIR model

- $S(t)$, $I(t)$, and $R(t)$ are the numbers of susceptible, infected, and removed individuals, respectively, at time t,
- μ is the natural birth and death rate,
- α is the infection rate,
- β is the recovery rate,
- γ is the reinfection rate,
- τ is the time delay after which recovered individuals become susceptible again.

In this model, the basic reproduction number R_0, which measures the average number of new infections caused by an infected individual, is given by:

$$R_0 = \frac{\alpha}{\beta + \mu}$$

When $R_0 > 1$, the infection spreads within the population.

4 Stability Analysis

To assess the model's stability, we identify equilibrium points by setting $\frac{dS}{dt} = \frac{dI}{dt} = \frac{dR}{dt} = 0$.

4.1 Disease-Free Equilibrium (DFE)

At the disease-free equilibrium, there are no infected individuals, so $I = 0$. This equilibrium point is given by:

$$(S^*, I^*, R^*)_{tr} = (N, 0, 0)$$

where the entire population remains susceptible. The DFE does not account for active infection dynamics and is therefore less relevant to epidemic analysis.

4.2 Endemic Equilibrium

The endemic equilibrium exists when $I \neq 0$ at finite times. This indicates a scenario where the infection persists within the population over time, creating periodic peaks without an eventual decline. We calculate the equilibrium as:

$$(S^*, I^*, R^*)_{ntr} = \left(\frac{\beta + \mu}{\alpha}, \frac{\mu N}{\beta + \mu} - \frac{\mu}{\alpha}, \frac{\beta N}{\beta + \mu} - \frac{\beta + \mu}{\alpha} + \frac{\mu}{\alpha} \right)$$

for $t < \tau$, and for $t \geq \tau$, the equilibrium becomes:

$$(S^*, I^*(t), R^*(t))_{ntr} = \left(\frac{\beta + \mu}{\alpha}, \frac{\mu N}{\beta + \mu} + \frac{\gamma I(t-\tau)}{\beta + \mu} - \frac{\mu}{\alpha}, \frac{\beta N}{\beta + \mu} - \frac{\beta + \mu}{\alpha} - \frac{\gamma I(t-\tau)}{\beta + \mu} + \frac{\mu}{\alpha} \right)$$

4.3 Jacobian Matrix and Eigenvalues

The Jacobian matrix J is constructed to analyze the stability around these equilibrium points:

$$J = \begin{bmatrix} -(\alpha I^* + \mu) & -\alpha S^* & 0 \\ \alpha I^* & \alpha S^* - \beta - \mu & 0 \\ 0 & \beta & -\mu \end{bmatrix}$$

The eigenvalues λ_0, $\lambda_\pm$ of J at the DFE are:

$$\lambda_0 = -\mu, \quad \lambda_+ = \alpha N - \beta - \mu, \quad \lambda_- = -\mu$$

The system behaves like a stable point when $\alpha < \frac{\beta+\mu}{N}$, similar to the classic SIR model. For general cases, the eigenvalues become complex if:

$$\alpha\beta > \frac{\alpha^2 (I^* - S^*)^2 + \beta^2}{2(S^* + I^*)}$$

indicating that $S(t)$, $I(t)$, and $R(t)$ oscillate around the equilibrium points.

5 Numerical Solution

Since the values of $S(t)$, $I(t)$, and $R(t)$ cannot be derived analytically from the set of differential equations in Eq. (1), we solve them numerically. The numerical solution reveals oscillatory behavior in $S(t)$, $I(t)$, and $R(t)$, with these variables exhibiting nearly constant-amplitude oscillations over time.

5.1 Observations from Oscillations

As shown in Fig. 3, the time series for $S(t)$, $I(t)$, and $R(t)$ displays multiple oscillatory waves. We observe that the average time period T of these oscillations is always greater than the delay parameter τ. This consistent pattern results from the conditions in Eq. (3). Since no damping factor is present in this model,

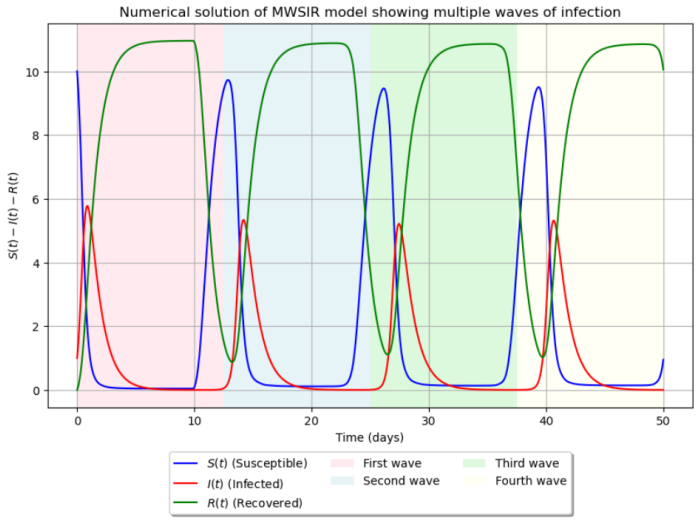

Figure 3: Four successive waves are shown here those are generated numerically by solving MWSIR model

the oscillation amplitudes do not decay over time, producing sustained waves in $S(t)$, $I(t)$, and $R(t)$.

The oscillations for $S(t)$, $I(t)$, and $R(t)$ share the same time period, though T gradually decreases with the number of cycles. The relative difference $T - \tau$ becomes negligible as τ increases. Figure 4 demonstrates this by plotting T and the relative difference $(T - \tau)/\tau$ as functions of τ.

5.2 Comparison with Real Data

The ongoing COVID-19 waves observed in India, represented in Fig. 1, display diminishing wave durations with $T_1 > T_2 > T_3$. The amplitude of the second wave is the highest, while the first wave shows the smallest amplitude. These observed characteristics indicate that the pandemic's progression in India is non-periodic.

To capture this non-periodic behavior, we further refine the MWSIR model by modifying parameters γ and τ. Specifically, we allow for time-dependent values:

$$\tau = \begin{cases} \tau_1, & t < \tau_2 \\ \tau_2, & t < \tau_3 \\ \tau_3, & t \geq \tau_3 \end{cases}, \quad \alpha = \begin{cases} \alpha_1, & 0 < t < \tau_2 \\ \alpha_2, & t \geq \tau_2 \end{cases}, \quad \gamma = \begin{cases} 0, & 0 < t < \tau_1 \\ \gamma_1, & \tau_1 \leq t < \tau_2 \\ \gamma_2, & t \geq \tau_2 \end{cases}$$

where the chosen parameter values are:

$$\tau_1 = 173, \quad \tau_2 = 440, \quad \tau_3 = 457, \quad \alpha_1 = 1.48 \times 10^{-7}, \quad \alpha_2 = 8.7 \times 10^{-7},$$

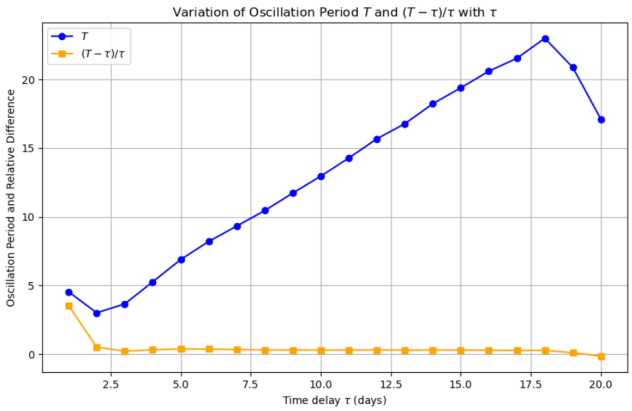

Figure 4: Variation of T and $T-\tau)/\tau$ with τ, in the MWSIR model

$$\gamma_1 = 0.055, \quad \gamma_2 = 0.08$$

Additionally, we set $\beta = \frac{1}{14}$ per day, reflecting a 14-day average recovery period. These parameter values are calibrated based on a single initial infection ($I(0) = 1$).

5.3 Model Fit and Interpretation

Using these parameter values, we solve the MWSIR model numerically and plot the results as red dashed lines in Fig. 6, alongside actual COVID-19 case data for India (blue solid line) over the same period. The model's outputs show a strong correlation with observed data, particularly in terms of wave timing and overall trend. Minor discrepancies, such as the first peak's overestimated height and the second peak's narrower width, may stem from variations in transmission rates for different viral strains.

The increase in α from α_1 to α_2 likely reflects the enhanced transmission potential of newer variants like Delta and Omicron, relative to the original SARS-CoV-2 strain.

To confirm the values of α_1 and α_2, we plot $S(t)$ and $I(t)$ in Fig. 7. The position of the infection peak can be identified by the relationship $S(t) = \frac{\beta}{\alpha}$. The first peak of $I(t)$ aligns with the crossing of $S(t)$ at the line $\beta/\alpha_1 = \frac{1}{14\times1.48\times10^{-7}} \approx 4.82625 \times 10^5$. Similarly, $S(t)$ intersects $\beta/\alpha_2 = \frac{1}{14\times8.7\times10^{-7}} \approx 8.21018 \times 10^4$ below the second and third peaks of $I(t)$.

The MWSIR model thus accurately identifies the dates of infection peaks as observed in the data, specifically on September 16, 2020; May 8, 2021; and January 25, 2022. Estimated heights for these peaks are:

$$I^{(1)}_{\max} = 1.07471 \times 10^5, \quad I^{(2)}_{\max} = 3.88941 \times 10^5, \quad I^{(3)}_{\max} = 2.57270 \times 10^5$$

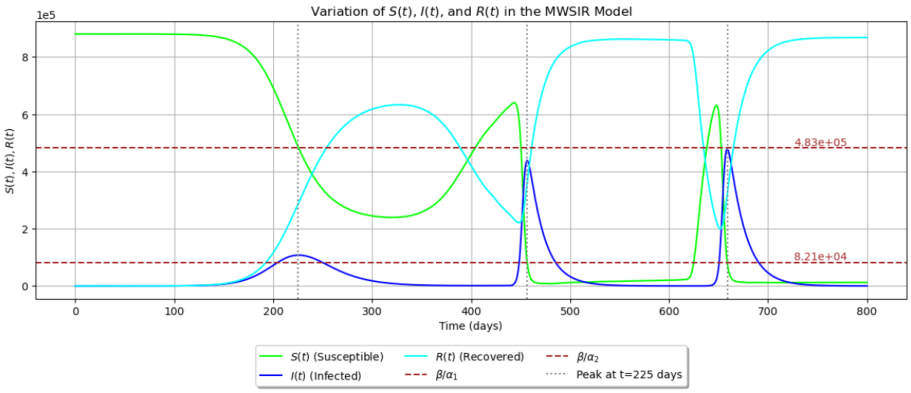

Figure 5: Geometric verification of α_1 and α_2 values using the intersection of $S(t)$ and horizontal lines at β/α

These values are within 17.52% of the actual peaks observed, demonstrating the robustness of the model.

5.4 Predictive Insights

This study suggests that 5.5% of individuals infected between January 30, 2020, and April 14, 2021, became susceptible to reinfection, while 8.0% of those infected later were reinfected. These results align with the estimated values of $\gamma_1 = 0.055$ and $\gamma_2 = 0.08$, indicating that measures like quarantine, isolation, and vaccination effectively reduce reinfection rates despite the emergence of more infectious variants.

Finally, as the MWSIR model's nonlinear equations are highly sensitive to initial conditions ($S(0)$, $I(0)$, $R(0)$), the values of α, γ, and τ may change with different starting conditions, which could alter subsequent predictions.

6 Conclusion

The MWSIR model successfully captures the periodic nature of infection waves, supported by stability analysis, which shows that equilibrium points can lead to oscillatory dynamics. This model aligns well with real-world data, providing a more comprehensive understanding of COVID-19 waves as observed in India.

References

[1] Kermack, N.O., McKendrick, A.G. "A Contribution to the Mathematical Theory of Epidemics." *Proceedings of the Royal Society of London A*, vol. 115, pp. 700-721, 1927.

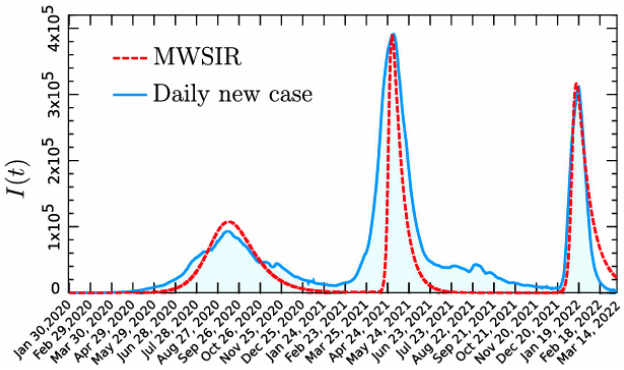

Figure 6: Daily new COVID-19 cases in terms of seven-day moving average in India during January 30, 2020 to March 14, 2022 (775 days) is compared with the numerical results obtained by the MWSIR model.

[2] Hethcote, H.W. "The Mathematics of Infectious Diseases." *SIAM Review*, vol. 42, pp. 599-653, 2000.

[3] Ghosh, K., Ghosh, A.K. "Study of COVID-19 Epidemiological Evolution in India with a Multi-Wave SIR Model." *Nonlinear Dynamics*, vol. 109, pp. 47-55, 2022.

[4] Keeling, M.J., Rohani, P. *Modeling Infectious Diseases in Humans and Animals*. Princeton University Press, 2008.